Carburization During Welding on Pressurized Natural Gas Pipelines

Andrei Artemev, John Goldak, Mihaela Mocanita,
Department of Mechanical and Aerospace Engineering
Carleton University, Ottawa, Ontario, K1S 5B6, Canada

Summary

While welding on a pressurized natural gas pipeline, the heat from the weld can cause localized carburization on the inner wall of an HSLA steel pipe. The carbon levels can exceed the eutectic composition of approximately 4.3 weight percent carbon in iron. This phenomena can produce a thin layer of liquid cast iron on the internal wall of the pipe directly under the welding arc. In this paper, this phenomena is simulated by the following method. The 3D transient energy equation is solved to compute the transient temperature field. While the temperature at a point on the internal pipe wall exceeds the eutectic temperature, it is assumed a thin layer of liquid exists. Further it is assumed that this layer grows by diffusion of carbon into the underlying solid. The limiting process is assumed to be the temperature dependent diffusion of carbon. A thermal-stress analysis computes distortion which can change the wall thickness and thus the temperature computed in the thermal analysis and the carburization analysis.

Introduction

Natural gas pipelines are welded under pressure for two reasons; to make a new connection to an existing pipeline or to repair damage such as that caused by corrosion [1]. If the pipeline is sufficiently thin, the part of the inner wall under the arc can reach temperatures approaching the melting point, 1530 ^{o}C for a typical HSLA pipeline steel. At these temperatures natural gas, which is mostly methane CH_4, can decompose by the reaction $CH_4 \rightarrow C + 2H_2$. The resulting carbon atoms react with the surface of the pipe. We conjecture that at temperatures above the eutectic temperature for this steel, 1147 ^{o}C, a very thin Fe–C film forms, perhaps only 1 to 2 atoms thick at first, and then the film grows by diffusion of carbon. The carbon diffuses into this film from the gas atmosphere, through the liquid film across the liquid-solid interface and into the solid. In this very thin film of liquid, it is assumed that advection, i.e., stirring or fluid flow effects, can be neglected. A film of such a brittle material increases the risk of cracking in the pipe. (The addition of hydrogen from the decomposition of natural gas adds to the concern. However, modelling the hydrogen behavior in this situation will be presented in a later publication.)

Displacement, strain and stress are computed by solving the conservation of linear momentum and mass equations. If the pressure and temperature are high enough, the wall thin enough and the time at temperature long enough, a groove can form under the weld by visco-plastic flow, i.e., creep. Such a groove changes the wall thickness and the distance from the bottom of the weld pool to the inner wall of the pipe and the temperature on the inner wall of the pipe. This will change the carburized layer thickness and composition. This coupling or interaction between thermal and stress analysis is an important nonlinear effect that has usually been neglected in CWM.

The paper is organized as follows: First the theory and numerical methods used are summarized. Then the results are described and conclusions stated.

Theory For Carburization Model

The temperature curves obtained at the points on the internal surface of the pipe were used to simulate the fluxing effect. The fluxing at the internal surface of the pipe was assumed to result from the absorption of carbon by the pipe material from the hydrocarbon rich environment inside the pipe. The increase in the carbon concentration results in melting starting at the internal surface of the pipe at temperatures significantly lower than solidus temperature corresponding to the nominal concentration of carbon in steel, $c_0 \approx 0.1\%$. We also assumed that the rate of carbon absorption is controlled by the diffusion through the growing liquid layer and that concentrations at the liquid-solid interface, $c_{\gamma L}$ and $c_{L\gamma}$, and liquid-gas phase interface, c_{L_0}, are determined by the equilibrium liquidus and solidus concentrations of Fe–Fe_3C diagram (Fig. 1). Therefore we neglected any effects of the melting kinetics and kinetics of the reaction between the gas phase and liquid material on the growth rate.

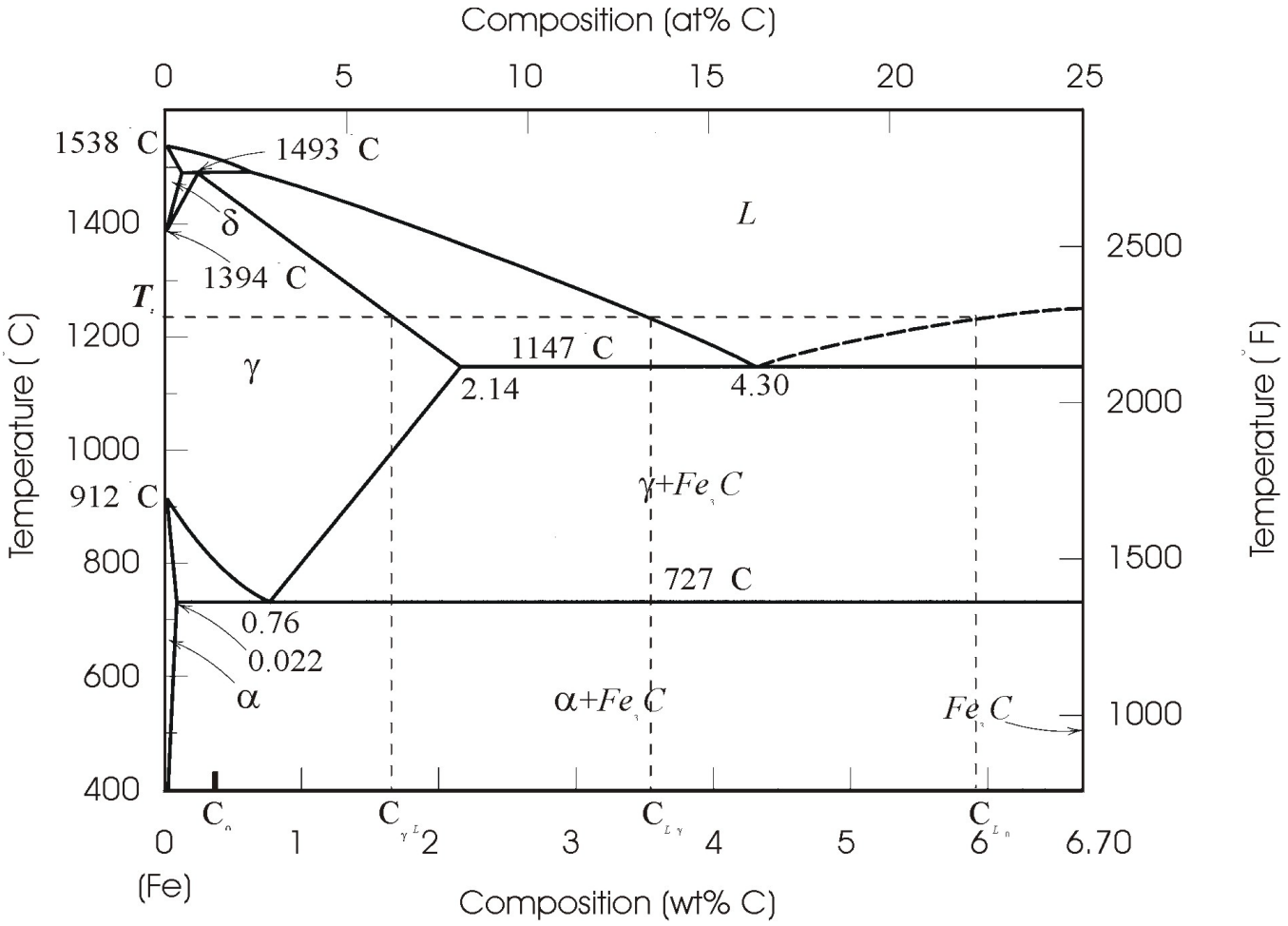

Figure 1: The iron iron carbide phase diagram with interface concentrations shown for liquid layer growing at temperature T_i.

It is possible to neglect the absorption of carbon by a solid material at a temperature below the eutectic temperature because the diffusivity of carbon in the solid phase is more than two orders of magnitude lower than the diffusivity of carbon in the liquid. As a result the overall contribution of gas to the solid phase transport into carburization is negligibly small compared to the contribution from the fluxing effect. In our model of the fluxing process we simulated the changes in the concentrations and phase state only at temperatures above the eutectic temperature. We assumed that an infinitesimally thin layer of the liquid phase is formed at the pipe internal surface at the moment when its temperature becomes higher than the eutectic temperature. After that the layer grows with the rate limited by the

diffusion of carbon from the liquid gas interface to the liquid solid interface. The boundary conditions for a corresponding diffusion problem and typical concentration distribution in the system during this process are illustrated in Fig. 2.

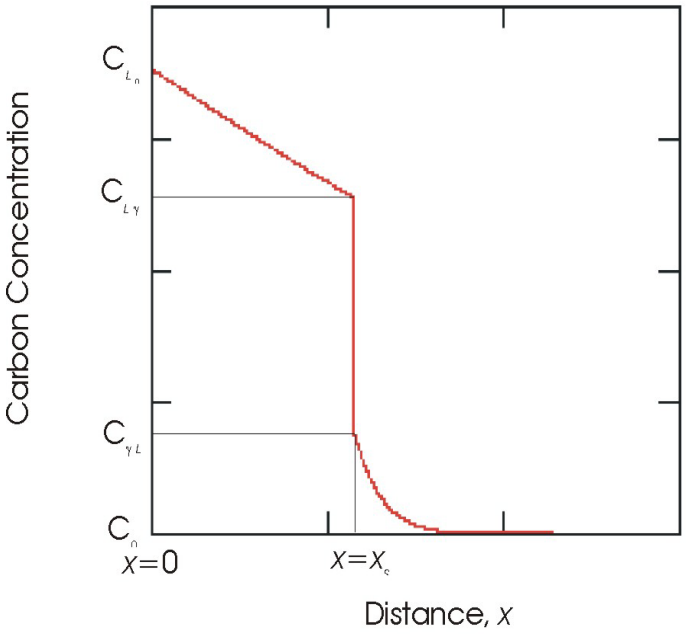

Figure 2: The distribution of the carbon concentration in the system with a liquid layer growing from the surface ($x = 0$). The liquid solid interface is located at x=xs.

An analytical solution exists for the diffusion problem with a constant growth temperature (constant values of c_{L_0}, $c_{L\gamma}$, and $c_{\gamma L}$)[2]. Under these conditions the thickness of the growing layer at time t can be found as:

$$x_s(t) \equiv 2\beta\sqrt{D_\ell t} \tag{1}$$

where the coefficient β is determined by the transcendental equation:

$$(c_{\gamma L} - c_{L\gamma})\sqrt{\pi}\beta = (c_{L\gamma} - c_{L0})\frac{\exp(-\beta^2)}{erf(\beta)} + (c_{\gamma L} - c_0)\frac{\sqrt{D_s}}{\sqrt{D_\ell}}\frac{\exp\left(\frac{-\beta^2 D_\ell}{D_s}\right)}{erf\left(\beta\frac{D_\ell}{D_s}\right)} \tag{2}$$

where D_ℓ and D_0 are diffusion coefficients of the liquid and solid phases, respectively ($D_\ell = 2.0 \times 10^{-8}$ m/s^2 and $D_0 = 1.0 \times 10^{-9}$ m/s^2 [3] was used). We used (1) and (2) to estimate the total thickness of the liquid layer which can be obtained under different welding conditions and to determine the size of mesh cells and number of cells in a mesh for the numerical solution of the diffusion problem with a varying growth temperature.

The numerical algorithm that has been used for the solution of the diffusion problem is based on the cellular model of the solidification process [4][5]. In this model space is divided into cells and every cell is characterized by a fraction of liquid, f_ℓ, and fraction of solid, $1 - f_\ell$, phases and carbon concentration in the liquid, c_ℓ, and/or in solid, c_s, phase. The size, Δx, and the number of cells in the

1-D mesh were estimated using (1) and (2) so that the liquid layer at the end of the growth process would consist of at least 10 cells and the total length of the mesh would be 2-3 times larger than the final thickness of the liquid layer. The diffusion transport is described in this model by an explicit finite difference scheme implemented separately for liquid and solid parts of the system. The solution for the concentration in liquid is evaluated only in the cells with a non-zero fraction of liquid, and the solution for the concentration in solid is evaluated in the rest of the system. The liquid and solid concentration fields overlap in one cell in which melting occurs and the fraction of liquid gradually increases. The length of time step, Δt, was limited by the stability criterion and by the solidification limit allowing not more than 0.1 of a cell to be solidified in one step.

Different boundary conditions were implemented at the external boundaries of the mesh and at the internal (liquid - solid) interface. The external boundaries had temperature (time) dependant Dirichlet type conditions c_{L0} and c_0 on liquid and solid sides of the mesh, respectively. The Neumann type condition was implemented in the melting cell with a zero transport from the liquid to solid phase and vice versa.

The evolution of a melting cell is determined by both diffusion and melting processes. At the beginning of the time step the concentrations in the liquid and solid phases in the melting cell are equal to $c_{L\gamma}$ and $c_{\gamma L}$, respectively. At every time step we calculate first the changes in the concentration in the solid and liquid phases in the melting cell using the diffusion equation. The zero liquid - solid diffusion exchange condition imposed on the melting cell (cell number i, cells with numbers $<$ i are liquid) results in the following changes in solid, Δc_s, and liquid, Δc_ℓ, concentrations produced by diffusion:

$$\Delta c_s = \frac{\Delta t \cdot D_s \cdot (c_s[i+1] - c_s[i])}{\Delta x^2 \cdot (1 - f_\ell)} \quad \text{and } \Delta c_\ell = \frac{\Delta t \cdot D_s \cdot (c_\ell[i-1] - c_\ell[i])}{\Delta x^2 \cdot f_\ell} \tag{3}$$

where $c_s[i]$ and $c_\ell[i]$ are concentrations in the solid and liquid phases in the cell number i. When these changes are added to concentrations, the updated values $c_s^+[i]$ and $c_\ell^+[i]$ differ from the equilibrium conditions at the liquid solid interface. $c_s^+[i]$ and $c_\ell^+[i]$ are used then to calculate the increase in fraction of liquid, Δf_ℓ, using the condition that at the end of a time step the equilibrium should be restored in the melting cell:

$$\Delta f_\ell = \frac{\left(c_\ell^+[i] - c_{L\gamma}\right) \cdot f_\ell + \left(c_s^+[i] - c_{\gamma L}\right)(1 - f_\ell)}{c_{L\gamma} - c_{\gamma L}} \tag{4}$$

At the end of a time step the fraction of liquid is updated using a calculated value of Δf_ℓ, and equilibrium values are assigned to concentrations in liquid and solid. If Δf_ℓ is such that an estimated fraction of liquid becomes larger than 1.0 then f_ℓ is assigned the value 1.0 and melting is transferred into the next cell. The fraction of liquid in the next cell is calculated so that the equilibrium interface conditions are established there. At the very beginning of melting we need to initialize melting in the first cell in the system when the temperature becomes just higher than the eutectic temperature. We do this by using equations (1) and (2) to estimate the thickness of liquid produced in such a first melting step. After that the described combination of diffusion steps and melting steps is used. The simulation is effectively terminated when the temperature curve drops below the eutectic temperature after passing through the maximum.

Thermal, Microstructure and Stress Analysis

The transient 3D energy equation is solved using 8-node bricks with backward Euler time integration. It is solved on the current deformed geometry for each time step. The thermal conductivity, and specific

enthalpy are assumed to be functions of temperature and microstructure. The weld pool size, shape and position and temperature distribution inside the weld pool is assumed to be known from experiment as a function of time. A convection coefficient of 1500 W/m^2K is assumed on the internal wall of the pipe due to the flowing natural gas. A convection coefficient of 10 W/m^2K for still air is assumed on the external surface of the pipe. The heating affect of the arc is described by a Dirichlet boundary condition on nodes in the weld pool. The temperature in a weld pool is assumed to vary parabolically from the melting point at the boundary of the weld pool to a maximum temperature of the melting point plus 400 ^{o}K at the weld pool centroid. Temperatures in the weld pool liquid/solid boundary were prescribed to 1800 ^{o}K. The maximum temperature in the weld pool was prescribed to 2200 ^{o}K. The size and shape of the weld pool was estimated from macrographs contained in [6].

The evolution of microstructure outside of the thin layer is computed using the methodology described in [7]. The microstructure evolution is assumed to be in equilibrium during heating, i.e., no super heating occurs. In austenite, grain growth begins after Nb and V carbo-nitrides dissolve and ceases when either delta ferrite forms on heating or ferrite, pearlite, bainite or martensite forms on cooling. Formation of ferrite, pearlite and bainite on cooling is modeled by ODEs. Martensite formation on cooling is modeled by the Koisten-Marburger equation.

The 3D transient nonlinear thermal stress analysis used a viscoplastic material model and 8-node bricks. Temperature dependent Young's modulus, Poisson's ratio, yield strength, hardening modulus and viscosity are used. Rigid body modes in the pipe were constrained. The loads, material properties and geometry are time dependent. The internal surface of the pipe was pressurized to 6.2 MPa. The transient temperature field of the thermal analysis was applied to each time step. The displacement, strain and stress were computed for 40 time steps for each weld, i.e., the weld moved approximately 2.5 mm in each time step. The stress analysis was done on the full vessel. See [8] for details on the thermal stress analysis.

The pipe was 508 mm diameter with a 7.9 mm wall of steel type API 5LX-65 ERW. See Figure 3. The data are taken from [6]. The welding consumables were Type E7018 low hydrogen shielded metal arc electrodes. At the test weld location a flat grove was machined into the pipe and a single weld pass was deposited along the centerline of the machined area. The weld was made with an internal pressure of 6.2 MPa. The welding current was 80 amps, the voltage 21 volts, the electrode size 2.38 mm, heat input 0.79 KJ/mm and travel speed 2.1 mm/s.

Conclusions and Acknowledgements

Figure 4 shows a typical transient temperature distribution with geometry deformed by stress analysis. Figure 5 shows the computed carbon concentration vs. distance from the internal wall at a point on the internal wall of the pipe. Figure 6 shows the thickness of the carburized film layer on several cross-sections vs. time. The dip in carbon concentration seen in Figure 6 corresponds to higher temperatures that shift the carbon concentration on the liquidus line to lower carbon values. The peak at the liquid-solid interface is caused by the temperature dropping to the eutectic temperature and that shifts the carbon level to the eutectic value. The results of our analysis are consistent with anecdotal evidence of a liquid carburized film forming on the inner wall of the pipe.

A model for predicting the formation of a carburized layer that forms on the inner wall of a pipe carrying natural during welding has been presented. The thickness of the liquid layer and the concentration of carbon as a function of distance from the inner wall of the pipe has been computed. A 3D transient temperature, displacement, stress and strain have been computed and coupled to the model for growth of the carburized layer.

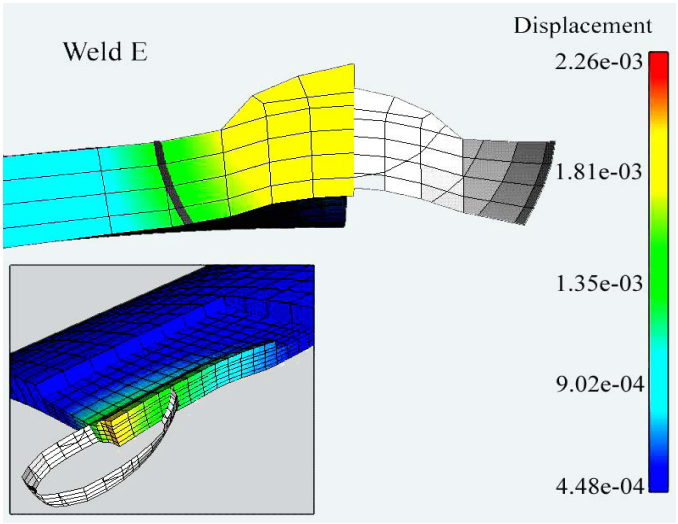

Figure 3: The 3D transient temperature field at a point in time just before the arc was extinguished is shown. The isosurface is for 1225 ^{o}K. Note the groove in the pipe that formed under the weld is due to creep driven by the internal pressure in the pipe.

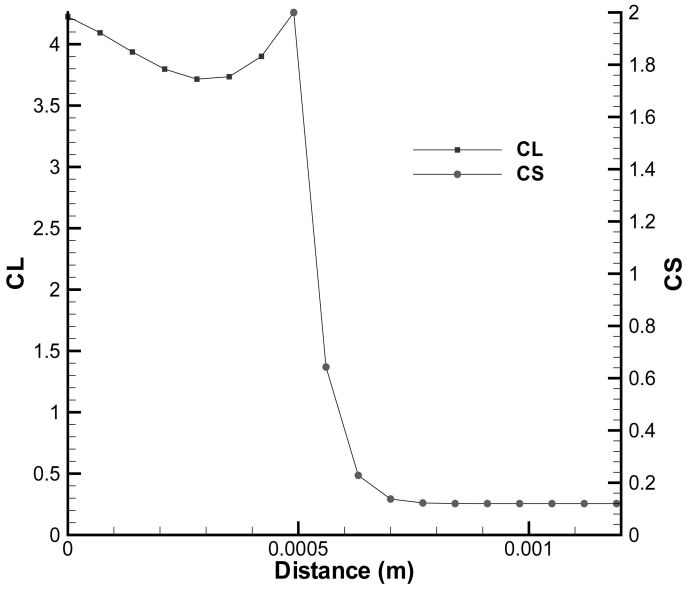

Figure 5: The carbon concentration distribution through the thickness of the liquid carburized film is shown at the point in time that the film growth stops. CL is the carbon concentration in liquid, CS is the carbon concentration in solid.

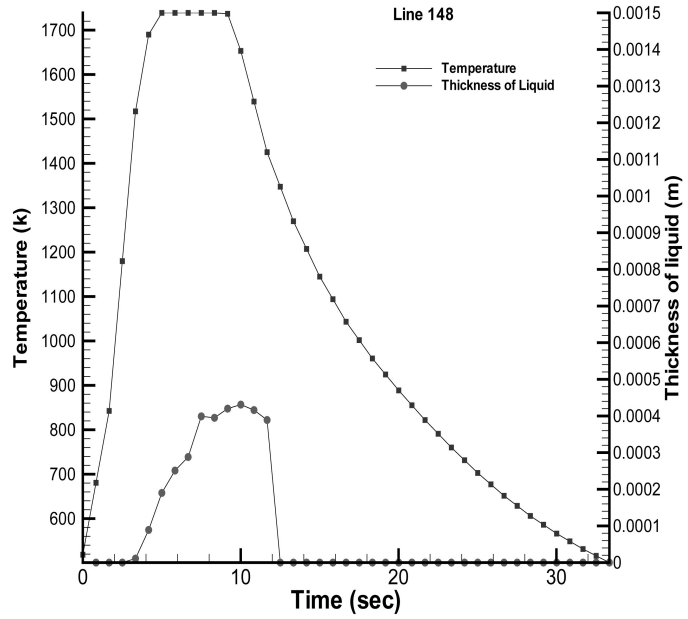

Figure 4: The temperature and thickness of the liquid layer versus time is shown for a point on the inside wall of the pipe.

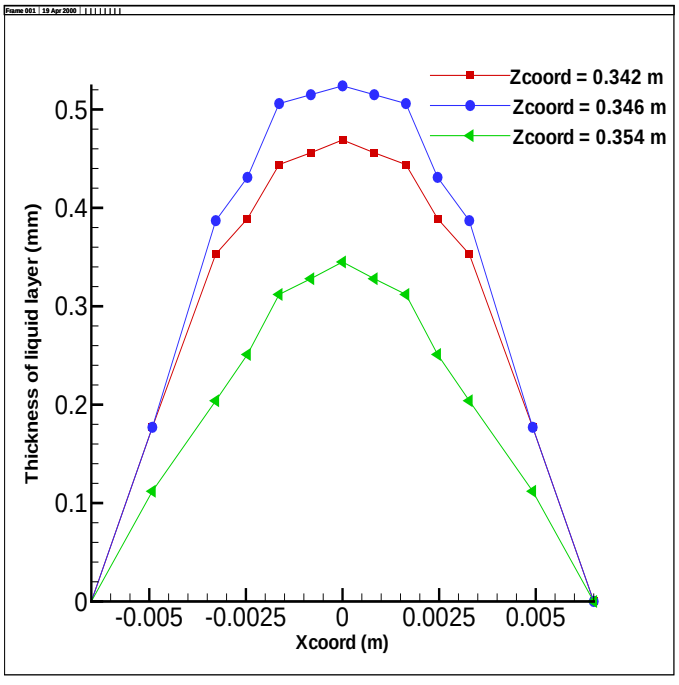

Figure 6: The thickness of the liquid layer as a function of distance from the weld centerline, Xcoord = 0, on the internal wall of the pipe. The thicker films are formed later in time and are downstream from the thinner films.

Acknowledgements

A. Artemev and J. Goldak thank the National Science and Engineering Research Council of Canada for financial support for this research.

References

[1] John Kiefner, *Effects of flowing products on line weldability*, Oil and Gas Journal, pp. 49-54, July 18, 1988.

[2] B. Liubov, *Diffuzionnye protsessy v neodnorodnykh tverdykh sredakh.* (in Russian: Diffusion Processes in Inhomogeneous Solids), Moscow, Nauka, 1981.

[3] W. Kurz and Fisher, *Fundamentals of Solidification*, Trans Tech Publications, Switzerland-Germany-UK-USA, 1989.

[4] A.R Umantsev, V.V. Vinogradov and V.T. Borisov. *Mathematical model of growth of dendrites in a supercooled melt.* Sov. Phys. Crystallogr. 30: # 3, 262-265, 1985.

[5] A. Artemev and J.A. Goldak. *Cellular simulation of the dendrite growth in Al-Si alloys.* Canadian Metall. Quart. 36: 57-64, 1997.

[6] PRC-185-9515, PRC Project No. August 3, 1995. *Repair of Pipelines by Direct Deposition of Weld Metal - Further Studies.*

[7] Henwood, C., Bibby, M.J., Goldak, J.A. and Watt, D.F., *Coupled Transient Heat Transfer-Microstructure Weld Computations (Part B)*, Acta Met., vol. 36, No. 11, pp. 3037-3046, 1988.

[8] J. Goldak, M. Mocanita, V. Aldea, J. Zhou, D. Downey, D. Dorling, *Predicitng Burn-Through When Welding on Pressurized Pipelines*, Proceedings of PVP'2000, 2000 ASME Pressure Vessels and Piping Conference, July 23-27, 2000, Seattle, Washington, USA.